THE JOURNAL OF PHYSICAL CHEMISTRY LETTERS
A JOURNAL OF THE AMERICAN CHEMICAL SOCIETY

pubs.acs.org/JPCL

Letter

Interpretations of High-Order Transient Absorption Spectroscopies

Peter A. Rose and Jacob J. Krich*

Cite This: J. Phys. Chem. Lett. 2023, 14, 10849−10855

Read Online

ACCESS | Metrics & More | Article Recommendations | Supporting Information

ABSTRACT: Transient absorption (TA) spectroscopy is an invaluable tool for determining the energetics and dynamics of excited states. When pump intensities are sufficiently high, TA spectra include both the generally desired third-order response and responses that are higher in order in the field amplitudes. Recent work demonstrated that pump-intensity-dependent TA measurements allow separating the orders of response, but the information content in those higher orders has not been described. We give a general framework for understanding high-order TA spectra. We extend to higher order the fundamental processes of standard TA: ground-state bleach (GSB), stimulated emission (SE), and excited-state absorption (ESA). Each order introduces two new processes: SE and ESA from previously inaccessible highly excited states and negations of lower-order processes. We show the new spectral and dynamical information at each order and show how the relative signs of the signals in different orders can be used to identify which processes dominate.

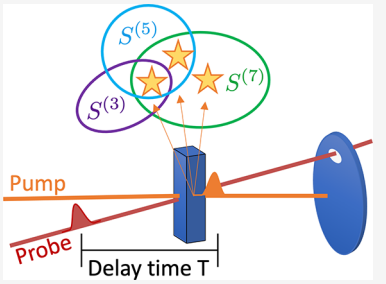

New forms of spectroscopy give new insights into the properties and dynamics of systems from atoms to solids. Linear absorption spectroscopy, in frequency ranges from THz to X-ray, gives information about the ground or thermal states of a material and its optically accessible excited states. Transient absorption (TA) spectroscopy measures the change in a probe pulse's absorption spectrum when it arrives a time T after a pump pulse, revealing both the absorption and dynamics of excited states.[1−13] The recently developed high-order transient absorption (HOTA) spectroscopy extends TA spectroscopy by systematically separating higher orders of nonlinear response, which has not previously been possible using TA methods.[14−16] These higher orders of nonlinear response contain information about energies, transition dipoles, and dynamics of multiply excited states.

TA signals with pump pulses that are not too strong can be intuitively understood in terms of three fundamental processes: excited-state absorption (ESA), stimulated emission (SE), and ground-state bleach (GSB).[17] There is a small probability that the pump excites the system into any of the available single-excitation states, which then evolve in time. When the probe arrives, the singly excited populations can undergo either SE back to the ground state or ESA up to doubly excited states. The population in the excited state is associated with a reduced population in the ground state, producing GSB, which is a reduction of the linear absorption from the level without the pump.

The TA signal $S(T, \omega)$ gives the change in the absorption of a probe pulse at frequency ω, which depends on the intensity of the pulses. Taking the electric dipole approximation and treating the fields classically, the standard interaction Hamiltonian is $H'(t) = -\mu\cdot\mathbf{E}(t)$, where $\mathbf{E}(t) = \mathbf{E}_a(t) + \mathbf{E}_b(t)$ is the electric field of the pump (a) and probe (b) pulses. We write $\boldsymbol{E}_j = \lambda_j[\boldsymbol{e}_j\varepsilon_j(t) + \boldsymbol{e}_j^*\varepsilon_j^*(t)]$, with $\boldsymbol{e}_j$ the polarization and $\varepsilon_j(t)$ containing the pulse amplitude, wavevector, and absolute phase. For our purposes, the key feature is the dimensionless λ_j, which scales the amplitude of the pulse. The typical third-order signal derives from a polarization field that is proportional to $\lambda_a^2\lambda_b$. We define the dimensionless pump intensity $I = \lambda_a^2$.

Moving beyond the lowest-order response, S can be expressed as a power series in I

$$S(T, \omega, I) = \overbrace{S^{(3)}(T, \omega)I}^{\text{standard TA signal}} + S^{(5)}(T, \omega)I^2 + S^{(7)}(T, \omega)I^3 + \ldots \quad (1)$$

Equation 1 assumes that the probe is weak and unchanging, and $S^{(n)}$ gives the nth-order material response, with only odd orders contributing to TA of samples large enough for phase matching.[17,18] Standard TA either chooses I small enough that the contributions beyond $S^{(3)}$ are negligible or has the higher-order contributions uncontrollably mixed with the lower-order ones, allowing study of I-dependent trends.[19−37] The new HOTA spectroscopy allows separating the $S^{(n)}$ at an intensity I_0 by combining TA spectra taken with N pump intensities

$$I_p = 4I_0\cos^2\left(\frac{\pi p}{2N}\right)$$

Received: September 5, 2023
Revised: November 13, 2023
Accepted: November 15, 2023

https://doi.org/10.1021/acs.jpclett.3c02491
J. Phys. Chem. Lett. 2023, 14, 10849−10855

for $p = 0, ..., N - 1$, where I_0 is chosen so that the contribution from $S^{(2N+3)}$ is negligible. The full method is described in refs 14 and 15.

The newly accessible HOTA spectroscopies contain information that has not previously been accessible in TA. This paper extends the standard ESA/SE/GSB pathways to higher orders, showing the spectral and dynamical information available in each new order in HOTA. We begin by discussing the dynamical information, which is easier to understand and serves as an intuitive starting place for discussing the higher-order signals. We then describe all of the Liouville pathways that exist for each order, introducing a nomenclature to discuss those contributions that is as useful as ESA/SE/GSB. We then describe the spectral information that exists in each order, focusing on two illustrative model systems.

We make a standard set of assumptions about the systems and light pulses under study. Before the pump arrives, the system is in a thermal state, ρ_{th}. We describe systems, as are commonly discussed in optical spectroscopy, with a ladder of dipole-allowed transitions, where n-times excited states are distinct from $(n + 1)$-times excited states, as indicated in the inset of Figure 1. We use $|n\rangle$ to refer to the set of n-times excited states and use $|n, \nu^{(n)}\rangle$ to refer to a particular state. Such an excitation ladder requires that the states $\{|n, \nu^{(n)}\rangle\}$ are long-lived with respect to the pump pulse duration. If this separation of time scales does not occur, eq 1 is still valid but much of the intuition developed in this paper is not directly applicable.

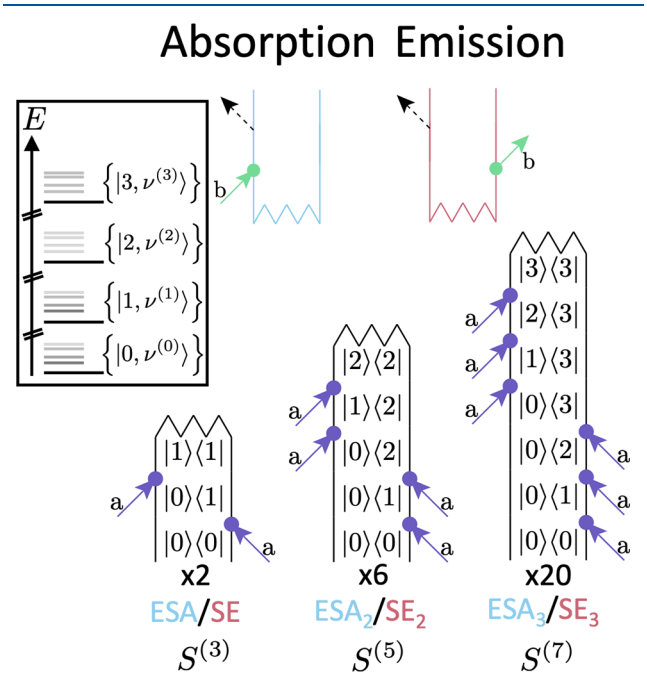

Figure 1. Sample Feynman diagrams for high-order processes broken into *bases* showing the action of the pump pulse, labeled "*a*", and *caps* showing the action of the probe pulse, labeled "*b*". Each base pairs with each cap, resulting in a complete Feynman diagram. Bases shown produce the highest possible number of excitations at third-, fifth-, and seventh-order, producing the ESA_n/SE_n diagrams with the appropriate cap. The multiplicative number under each base indicates the number of similar bases formed by permutation of the ordering of the pump arrows, confirmed with an automated diagram generator.[42] The excitation numbers are not shown in the caps since the caps pair with every base and because n can change due to relaxation during the delay time T. Inset: Sample ladder-type spectrum, with 0-, 1-, 2-, and 3-excitation states shown.

Each signal $S^{(2n+1)}(T)$ in eq 1 can contain the dynamics of at most n-times excited states. This intuitive claim follows from the excitation ladder model and the TA phase-matching condition.[17,38] We illustrate it using double-sided Feynman diagrams to describe the pathways that contribute to $S^{(2n+1)}$. We assume that the probe is weak, so there is only one interaction with the probe; the remaining $2n$ interactions are with the pump, and the two pulses do not overlap in time. TA phase matching requires that there be equal numbers of left- and right-directed pump interactions, representing the $\mathcal{E}_a$ and $\mathcal{E}_a^*$ terms in the field, and the rotating wave approximation (RWA) requires that arrows directed in cause excitations while arrows directed out cause de-excitations.[17,38] Then the highest excitation states that can be reached after the pump occur when the raising operator is applied n times to both the bra- and ket-sides of the initial density matrix, which requires $2n$ interactions. We divide the Feynman diagrams into *bases* that involve only interactions with the pump pulse and two *caps* that involve only one interaction with the probe, as shown in Figure 1, with a full diagram formed by combining any base with either cap. The bases shown in Figure 1 represent the highest-excitation pathways available at the third, fifth, and seventh order. Lower excitation pathways also exist, and we discuss them below. In Figure 1, the label $|n\rangle\langle m|$ is a placeholder for a density matrix $\sum_{jk} c_{jk} |n, \nu_j^{(n)}\rangle\langle m, \nu_k^{(m)}|$.

We generalize the concept of stimulated emission and excited-state absorption from the singly excited states to similar processes that originate from the n-excitation states. When the $S^{(3)}$ bases shown in Figure 1 are combined with the absorption (emission) cap, we obtain the familiar ESA (SE) pathway. By analogy, when the $S^{(5)}$ bases are combined with the absorption (emission) cap, we obtain a conceptually similar type of signal, which is excited-state absorption or stimulated emission from the doubly excited states. We call these pathways ESA_2/SE_2 for $S^{(5)}$ and ESA_n/SE_n for higher orders. These two pathways contain all of the new dynamical information that is revealed at the order $(2n + 1)$. When T is greater than the lifetime of the n-times excited states, the n-times excited population decays during the waiting time, and the $ESA_n(SE_n)$ pathways include absorption (emission) processes beginning from lower-excitation states. Such decays generally change the signal, allowing those lifetimes to be determined.[14] Each HOTA signal also involves contributions from pathways with lower numbers of excitations immediately after the pump. Those pathways have dynamical information that generally already exists in lower-order signals, although interferences of the type discussed below could mask the signal in lower orders. The exception to this rule occurs at third order, where GSB, which is a negation of linear absorption, also introduces ground-state vibrational dynamics that were not present in the static linear absorption signal. As usual, care must be taken in assigning physical significance to pathways. For example, in a two-level system with relaxation, there is no physical excited-state absorption process. However, the ESA pathway must still be calculated because after the pump pulse excites the system, the system relaxes to the ground state. The probe pulse can then excite the system again. The dynamical information about the lifetime of the excited state is still captured in the SE/ESA pathways.

Since each order controllably adds a single set of excitation states not in the lower-order signals, new dynamics in higher

https://doi.org/10.1021/acs.jpclett.3c02491
J. Phys. Chem. Lett. 2023, 14, 10849−10855

orders can immediately be attributed to new processes. One can analyze each order sequentially, beginning from third order, and characterizing the decay constants (e.g., using global analysis[39−41]) and beat frequencies associated with each order. If the fifth-order signal contains the same decay constants and frequencies as the third-order and also contains a new set of dynamics, those new dynamics can be attributed to processes involving only the twice excited states $|2, \nu^{(2)}\rangle$, and analogously for higher orders. For example, in the semiconductor case, new decays in systems with multiple excitations are called Auger processes, and they have been long studied with intensity-dependent transient absorption.[19] Auger processes in excitonic systems require either an exciton and another free charge or two excitons. In a system in which one optical absorption produces only one exciton and where there are no other background carriers or excitons, the third-order HOTA signal cannot have any Auger decays. In that same system, the fifth-order SE_2 and ESA_2 can show Auger-like decays from two-exciton states. Alternatively, systems with carrier multiplication, where one optical absorption can produce multiple excitons, or with background carriers (e.g., from dopants) can have Auger processes at third order.

We now consider the full set of pathways contributing to TA signals at all orders. We build an understanding by comparing the well-known third-order signal to the linear absorption signal (A). Standard third-order TA involves two new processes involving singly excited states after the pump (ESA/SE) and a negation of the linear absorption (GSB). In order to generalize to higher orders, we also refer to GSB as negated absorption ($NA^{(3)}$). This labeling introduces a pattern that applies at higher orders: the $(2n + 1)$-order signal introduces two new processes (ESA_n/SE_n) and negations of all lower-order processes, which we illustrate in Table 1 and now describe.

Table 1. Names of Pathways in (Transient) Absorption Spectroscopy to the Seventh Order[a]

	Optical excitations after pump			
Order	0	1	2	3
1	+ **A**			
3	$-NA^{(3)}$	+ **ESA**		
	(GSB)	− **SE**		
5	+ $A^{(5)}$	$-NESA^{(5)}$	+ $\mathbf{ESA_2}$	
		+ $NSE^{(5)}$	− $\mathbf{SE_2}$	
7	$-NA^{(7)}$	+ $ESA^{(7)}$	$-NESA_2^{(7)}$	+ $\mathbf{ESA_3}$
		− $SE^{(7)}$	+ $NSE_2^{(7)}$	− $\mathbf{SE_3}$

[a]The ± shows the sign of the pathway's contribution. Pathways representing new dynamical information are in bold and appear along the diagonal. Pathways left of the diagonal negate (with the letter N) or revive pathways that first appeared at lower orders. Superscript shows the order of the contribution, which is suppressed for the diagonal contributions.

Next we compare the fifth- and third-order signals. The fifth-order signal contains new information about the two-excitation states in the ESA_2/SE_2 pathways shown in Figure 1. It also includes processes that can be interpreted as negations of the signals associated with the 1-excitation states, which we call negated excited-state absorption (NESA) and negated stimulated emission (NSE), shown diagrammatically in Figure 2. Intuitively these negations occur because the fifth-order response involves moving population from the 1-excitation states that produce ESA/SE to the 2-excitation states as well as back to the 0-excitation states. That increase in ground-state population gives an increase in the linear-absorption-type process (undoing part of the GSB), which we call $A^{(5)}$.

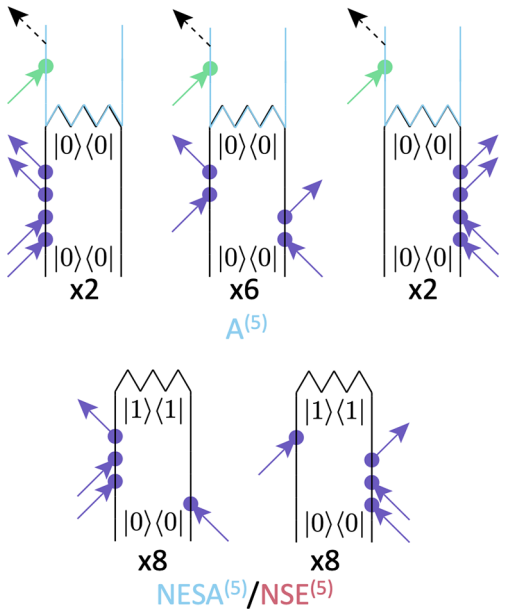

Figure 2. Pathways contributing to $S^{(5)}$ that negate third-order processes. Top row shows contributions to increased ground-state absorption and includes the absorption cap. Second row shows bases associated with the negation of the third-order ESA and SE pathways. All 16 bases contribute to $NESA^{(5)}$ ($NSE^{(5)}$) when paired with the absorption (emission) cap shown in Figure 1. The number of similar permutations of the pump interactions is given below each diagram. The diagrams associated with ESA_2/SE_2 are displayed in Figure 1.

We can extend this pattern and nomenclature to any order, which we demonstrate by comparing the seventh- and fifth-order signals. The new information in seventh order is contained in the ESA_3/SE_3 processes, which report on the 3-excitation states. The seventh-order signal also includes negations of those in the fifth-order pathways, with the relevant bases shown in Figure 3. The seventh-order signal includes negations of the ESA_2/SE_2 pathways, which we call $NESA_2^{(7)}/NSE_2^{(7)}$, a contribution to the ESA/SE-type processes, which have the same signs as the originals and which we call $ESA^{(7)}/SE^{(7)}$, and a negation of the absorption process, which we call $NA^{(7)}$.

Each higher-order signal contains pathways that are related to the pathways at the previous order but have opposite signs, as shown on the subdiagonal of Table 1.We gave the intuitive explanation for these alternating signs; diagrammatically, the alternation can be understood by analyzing the bases in Figures 1−3. Each signal $S^{(2m+1)}$ is proportional to a factor of $(-i)^{2m+2}$, so every signal order $S^{(2m+1)}$ has an overall factor of $i^2 = -1$ as compared with $S^{(2m-1)}$.[17] In addition, every arrow that occurs on the bra side of the diagrams gives a factor of −1. Combining these two rules gives the conclusion that ESA_n has the same sign for all n, and similarly that SE_n has the same sign for all n. However, all of the diagrams that correspond to signals that existed in the lower order involve adding an even number of arrows to the bra side of the diagram, as compared to the previous order. Therefore, all of these diagrams contribute the opposite sign relative to their previous-order counterparts. The Supporting Information contains a discussion of modifications

https://doi.org/10.1021/acs.jpclett.3c02491
J. Phys. Chem. Lett. 2023, 14, 10849−10855

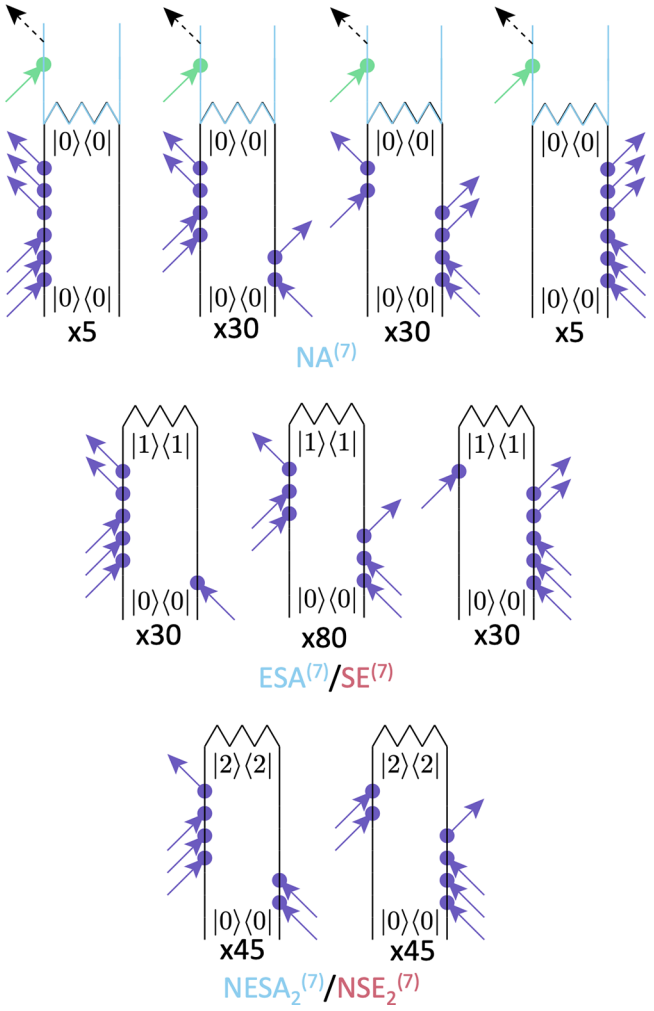

Figure 3. Pathways contributing to $S^{(7)}$ that negate fifth-order processes. The top row shows contributions to negated ground-state absorption and includes the absorption cap. The second row shows bases associated with the increase of the third-order ESA and SE processes. The third row shows bases associated with the negation of the fifth-order ESA_2 and SE_2 processes. The number of similar permutations of the pump interactions is below each diagram. The bases associated with ESA_3/SE_3 are displayed in Figure 1.

that are required when pump or probe photon energies are close to the thermal energy, e.g., with THz spectroscopies, as well as a discussion of the permutations of the diagrams shown in Figures 1−3.

One approach to calculating and understanding TA spectra with intense laser pulses involves solving the equations of motion for the system including the effects of the pulse fields, which is not a perturbative approach.[10] Within this context, ref 32 describes a method for calculating nonperturbative response functions for two-level electronic systems coupled to vibrational degrees of freedom. These nonperturbative response functions provide an efficient method for calculating the summation of terms $(N)A^{(2n+1)}I^n$ and $(N)SE^{(2n+1)}I^n$ for a given pulse intensity.

To demonstrate some of the new information about transition dipoles and energies of high-excitation states present in HOTA, we introduce two model systems. The first is a ladder model with Hamiltonian

$$H_0 = \hbar \begin{pmatrix} 0 & 0 & 0 & 0 & 0 \\ 0 & \omega_1 & 0 & 0 & 0 \\ 0 & 0 & \omega_2 & 0 & 0 \\ 0 & 0 & 0 & \omega_3 & 0 \\ 0 & 0 & 0 & 0 & \omega_4 \end{pmatrix} \tag{2}$$

and dipole operator

$$\mu = \begin{pmatrix} 0 & \mu_{10} & 0 & 0 & 0 \\ \mu_{10} & 0 & \mu_{21} & 0 & 0 \\ 0 & \mu_{21} & 0 & \mu_{32} & 0 \\ 0 & 0 & \mu_{32} & 0 & \mu_{43} \\ 0 & 0 & 0 & \mu_{43} & 0 \end{pmatrix} \tag{3}$$

We take $\mu_{n,n-k}$ for $k > 1$ to be zero because we assume that the pulse bandwidth does not support such transitions. The frequency differences $\omega_{n,n-1} \equiv \omega_n - \omega_{n-1}$ are the spectral locations where peaks may appear. Note that this excitation ladder model contains no dynamics, so the signal $S^{(2n+1)}$ is constant for $T > 0$, in the impulsive limit. This model could represent an anharmonic vibrational mode of a molecule, which might be studied using IR pump and probe pulses.[38] The purpose of this discussion is to paint a general picture of the kinds of spectral information that can be revealed (or hidden) in HOTA spectra regardless of the wavelength or sample type.

At each order, new spectral information is revealed by the ESA_n process, which reports on energetic transitions that were inaccessible at the previous order. As long as the new energetic transitions are distinct from previous transitions, this new information appears in spectra as new positive-signed peaks. To illustrate this idea, we show simulated spectra for an unequally spaced ladder model in Figure 4, for which we use $\{\omega_1, \omega_2, \omega_3, \omega_4\} = \{1, 1.9, 2.7, 3.4\}\omega_0$ and have assumed that the excitation energies are larger than the thermal energy, with simulations using the open-source ultrafast spectroscopy suite (UFSS).[42−44] We take all $\mu_{n,n-1} = 1$ and simulate a closed system with no relaxations, with all of the peaks given the same phenomenological line widths for visualizing the spectra. In the impulsive limit, the peak heights are fully determined by the dipole transition strengths $\mu_{n,n-1}$ (see Tables S2 and S3 for examples), and we show below how this fact can be used to determine which signal types are dominant when the transition energies are degenerate. The peak at ω_{10} corresponds to linear absorption at first-order, GSB/SE at third order, and the negations/revivals of these processes at higher orders. The sign of the peak at ω_{10} flips with each order. In addition, each order reveals a new spectral peak, corresponding to ESA at the third order and ESA_n at higher order. Peaks at the same spectral positions appear at higher orders, again with alternating sign.

When spectral peaks overlap, interpreting the spectra becomes more complicated. Such overlaps have complicated the interpretation of high-order TA signals, for example in quantum dots, requiring careful analysis to untangle.[30] To build intuition, we move to a degenerate ladder model in which the ESA_n/SE_n processes are all at the same frequency and allow μ in eq 3 to vary. In the Supporting Information we derive expressions for the third- and fifth-order signals using a

https://doi.org/10.1021/acs.jpclett.3c02491
J. Phys. Chem. Lett. 2023, 14, 10849−10855

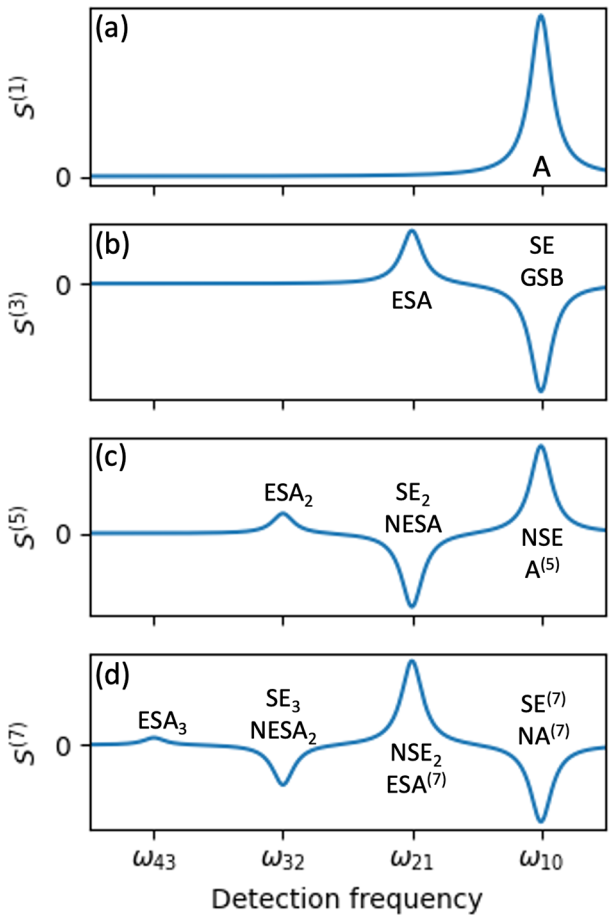

Figure 4. Simulated spectra of an anharmonic ladder for (a) linear absorption, (b) standard (third-order) TA, (c) fifth-order TA, and (d) seventh-order TA. The ESA_n process is the lowest-energy peak in each spectrum and always contributes with a positive sign. All spectral features from one spectrum appear with a negative sign in the next spectrum.

model with no 3-excitation states ($\mu_{32} = 0$) and with $\omega_{10} = \omega_{21} = \omega_0$. We see that

$$S^{(3)}(T, \omega_0) \propto -2\mu_{10}^4 + \mu_{21}^2\mu_{10}^2 \tag{4}$$

$$S^{(5)}(T, \omega_0) \propto -\frac{1}{12}(7\mu_{21}^4\mu_{10}^2 - \mu_{21}^2\mu_{10}^4 - 8\mu_{10}^6) \tag{5}$$

In this case, the third-order signal vanishes when $\mu_{21} = \sqrt{2}\mu_{10}$, whereas the fifth-order signal vanishes when $\mu_{21} = \sqrt{8/7}\mu_{10}$, assuming that all processes give the same lineshapes. In the range $\sqrt{8/7} < \mu_{21} < \sqrt{2}$, both the third- and fifth-order signals are negative, breaking the expected pattern of alternating signs that appears in Figure 4. Note that, for a harmonic vibrational mode, $\mu_{21} = \sqrt{2}\mu_{10}$, and the third-order peak vanishes.[3] A third-order peak that vanishes due to such interferences between pathways is not unique to harmonic modes, and we demonstrate below how a simple biexciton model may produce the same effect.

If a negative-signed peak appears in both the third- and fifth-order signals at short T, it indicates overlap of transitions to 1- and 2-excitation states. Negative peaks in third-order signals originate in GSB/SE processes between the 0- and 1-excitation states. Looking at Table 1, the only negative contributions to $S^{(5)}$ are SE_2 and $NESA^{(5)}$, which both occur at the same spectral positions: transitions between 1- and 2-excitation states. The fifth-order negations of the GSB/SE processes have positive signs, so if the fifth-order signal at the same spectral position is also negative, it indicates the presence of a hidden ESA process at third order and indicates that the dipole contributing to that ESA pathway, μ_{21}, cannot be too large. In this case, the fifth-order spectra gives new spectral information about 1-excitation states, as we found in the study of quantum dots in ref 14.

As an interesting limiting case, if a peak at some frequency first appears in $S^{(5)}$ and it has a negative amplitude, it reveals a dipole-allowed transition between both $|0\rangle \rightarrow |1\rangle$ and $|1\rangle \rightarrow |2\rangle$ that are normally visible in third order but cancel each other. This situation is in contrast to a peak that first appears in $S^{(5)}$ with a positive sign, which reports on transitions between $|2\rangle$ and $|3\rangle$ states, as discussed above. In our simple model, a new negative peak demonstrates that μ_{21} must be roughly $\sqrt{2}$ stronger than μ_{10}.

This phenomenon of 1-excitation pathways canceling in the third-order signal while appearing in the fifth-order signal can occur in many situations, and we now introduce a model of optical spectroscopy of biexcitons to illustrate another simple case. Let $a_A^\dagger$ and $a_B^\dagger$ create excitons and let the Hamiltonian be

$$H_0 = \hbar \sum_{i=A,B} a_i^\dagger a_i \omega_i + J(a_A^\dagger a_B + \text{h.c.})$$

where $\hbar$ is Planck's constant and J is the coupling between the two bare excitons with energies $\hbar\omega_i$. The ground-state energy is $\hbar\omega_g = 0$, and the biexciton has the energy $\hbar\omega_{AB} = \hbar(\omega_A + \omega_B)$. We set the dipole transitions for each bare exciton equal, that is, $\mu_{g,A} = \mu_{g,B} \equiv \mu_0$, and similarly $\mu_{A,AB} = \mu_{B,AB} = \mu_0$, which is different from the previous ladder model, in which the third-order signal vanished only if $\mu_{21} = \sqrt{2}\mu_{10}$. Let $\hbar\omega_\alpha$ and $\hbar\omega_\beta$ be the eigenenergies of the single exciton states, with corresponding transition dipoles $\mu_{g,\alpha}$, $\mu_{g,\beta}$, $\mu_{\alpha,AB}$, and $\mu_{\beta,AB}$. Tuning J modifies the single exciton eigenstates and, crucially, $\mu_{g,\alpha}$, $\mu_{g,\beta}$, $\mu_{\alpha,AB}$, and $\mu_{\beta,AB}$.[45]

When the ratio of dipole couplings is correct, the third-order signal at ω_α can be found to cancel, as demonstrated in Figure 5. When $J = 0.18\hbar(\omega_B - \omega_A)$, the third-order signal at ω_α vanishes, while there is a negative fifth-order signal. As in the ladder model, the new negative feature in the fifth order cannot be an ESA_2 contribution but instead reports on 1-excitation signals that were masked in the third order. The same phenomenon can also occur in a model with $J = 0$ but fast relaxation from $|B\rangle$ to $|A\rangle$.[14] In both realizations of the biexciton model, one of the two exciton peaks is invisible at the third order and appears as a negative peak in the fifth-order signal. The simplicity of the two quite different parameter regimes under which this phenomenon appears underscores the fact that this phenomenon can occur in a wide range of systems.

This discussion emphasizes the value of measuring simultaneously both $S^{(3)}$ and $S^{(5)}$, and it shows some of the information that can be revealed by comparing the two signals. We draw particular attention to the fact that comparing the signs of peaks in third- and fifth-order signals immediately reveals the nature of the dominant signal at each spectral location.

Many methods have been used or proposed to extract different high-order responses, frequently involving more than

https://doi.org/10.1021/acs.jpclett.3c02491
J. Phys. Chem. Lett. 2023, 14, 10849−10855

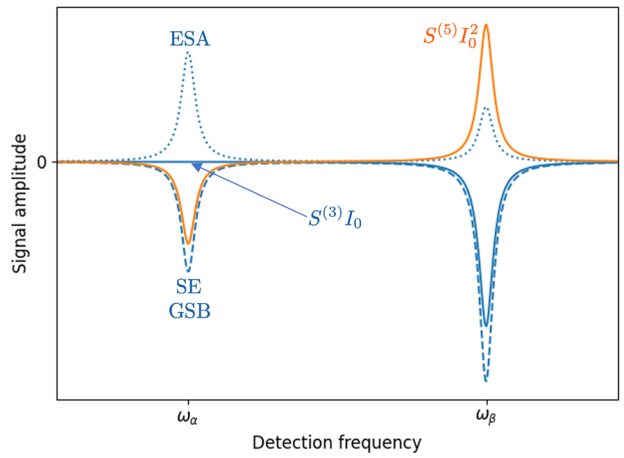

Figure 5. HOTA spectra for a model where the lower exciton peak vanishes at third order (solid blue) and is negative at fifth order (orange). The negative-signed GSB + SE signals (dashed) precisely cancel the positive-signed ESA signal (dotted). Here $J = 0.18(\omega_\beta - \omega_\alpha)$ and there is no relaxation.

two pulses.[16] References 46 and 47 discuss 3-pulse experiments that are high-order extensions of double-quantum (HODQ) spectroscopy.[48] Both HOTA and HODQ extract the emission/absorption lineshapes for higher-lying excited states. HOTA also extracts population dynamics for high-lying excited states. In contrast, HODQ does not extract any population dynamics but rather extracts the frequency−frequency correlation between excitation and emission at a population time of 0. HOTA is experimentally simpler because it requires only a standard TA setup, whereas HODQ requires three pulses and phase-matching or phase-cycling routines. HODQ has the advantage of being background-free, as there is only a signal if higher-lying excited states exist.[47] In contrast HOTA always has nonvanishing signals $S^{(2n+1)}$ for all n, even if the system only supports a single dipole-allowed transition. There are also other methods for measuring higher-order responses such as exciton−exciton interaction 2D spectroscopy (EEI2D), a fifth-order signal that gives excitation and emission/absorption lineshapes, as well as population dynamics, but is again more experimentally challenging than HOTA.[49] Both HODQ and EEI2D potentially suffer from higher-order contaminations, which can be difficult to quantify. One of the key advantages offered by HOTA is the clean separation of nonlinear orders.

We have laid the foundation for understanding the higher-order perturbative terms that can now be measured using the method outlined in ref 14. We introduced a language to describe the processes contributing to these higher-order signals and used two simple models to illustrate the new kinds of spectral information that can be uncovered by comparing the third- and fifth-order signals. In particular, we showed that new peaks emerging at fifth-order reveal new spectral information if the peak is positive or reveal previously hidden spectral information if the peak is negative.

■ ASSOCIATED CONTENT

Supporting Information

The Supporting Information is available free of charge at https://pubs.acs.org/doi/10.1021/acs.jpclett.3c02491.

Extension of HOTA to include THz pump and probe pulses at finite temperature, discussion about how to enumerate all Feynman diagrams that contribute to HOTA signals, and derivation of eqs 4 and 5 (PDF)

Transparent Peer Review report available (PDF)

■ AUTHOR INFORMATION

Corresponding Author

Jacob J. Krich − *Department of Physics and Nexus for Quantum Technologies, University of Ottawa, Ottawa ON K1N 6N5, Canada;* orcid.org/0000-0003-4514-0720; Email: jkrich@uottawa.ca

Author

Peter A. Rose − *Department of Physics, University of Ottawa, Ottawa ON K1N 6N5, Canada;* orcid.org/0000-0003-0956-944X

Complete contact information is available at: https://pubs.acs.org/10.1021/acs.jpclett.3c02491

Notes

The authors declare no competing financial interest.

■ ACKNOWLEDGMENTS

We acknowledge helpful conversations with Tobias Brixner, Pavel Malý, and Julian Lüttig and a careful reading by Julian Lüttig. We acknowledge funding from the Natural Sciences and Engineering Research Council of Canada.

■ REFERENCES

(1) Jonas, D. M.; Bradforth, S. E.; Passino, S. A.; Fleming, G. R. Femtosecond Wavepacket Spectroscopy: Influence of Temperature, Wavelength, and Pulse Duration. *J. Phys. Chem.* **1995**, *99*, 2594−2608.

(2) Berera, R.; van Grondelle, R.; Kennis, J. T. M. Ultrafast Transient Absorption Spectroscopy: Principles and Application to Photosynthetic Systems. *Photosynth. Res.* **2009**, *101*, 105−118.

(3) Hamm, P. Femtosecond IR Pump-Probe Spectroscopy of Nonlinear Energy Localization in Protein Models and Model Proteins. *J. Biol. Phys.* **2009**, *35*, 17−30.

(4) Ohkita, H.; Ito, S. Transient Absorption Spectroscopy of Polymer-Based Thin-Film Solar Cells. *Polymer* **2011**, *52*, 4397−4417.

(5) Cho, B.; Tiwari, V.; Hill, R. J.; Peters, W. K.; Courtney, T. L.; Spencer, A. P.; Jonas, D. M. Absolute Measurement of Femtosecond Pump−Probe Signal Strength. *J. Phys. Chem. A* **2013**, *117*, 6332−6345.

(6) Maiuri, M.; Garavelli, M.; Cerullo, G. Ultrafast Spectroscopy: State of the Art and Open Challenges. *J. Am. Chem. Soc.* **2020**, *142*, 3.

(7) Pandya, R.; Chen, R. Y. S.; Gu, Q.; Gorman, J.; Auras, F.; Sung, J.; Friend, R.; Kukura, P.; Schnedermann, C.; Rao, A. Femtosecond Transient Absorption Microscopy of Singlet Exciton Motion in Side-Chain Engineered Perylene-Diimide Thin Films. *J. Phys. Chem. A* **2020**, *124*, 2721−2730.

(8) Provazza, J.; Segatta, F.; Coker, D. F. Modeling Nonperturbative Field-Driven Vibronic Dynamics: Selective State Preparation and Nonlinear Spectroscopy. *J. Chem. Theory Comput.* **2021**, *17*, 29−39.

(9) Cina, J. A. *Getting Started on Time-Resolved Molecular Spectroscopy*; Oxford University Press, 2022.

(10) Gelin, M. F.; Chen, L.; Domcke, W. Equation-of-Motion Methods for the Calculation of Femtosecond Time-Resolved 4-Wave-Mixing and N-Wave-Mixing Signals. *Chem. Rev.* **2022**, *122*, 17339−17396.

(11) Xu, C.; Lin, K.; Hu, D.; Gu, F. L.; Gelin, M. F.; Lan, Z. Ultrafast Internal Conversion Dynamics through the On-the-Fly Simulation of Transient Absorption Pump−Probe Spectra with Different Electronic Structure Methods. *J. Phys. Chem. Lett.* **2022**, *13*, 661−668.

(12) Unger, F.; Moretti, L.; Hausch, J.; Bredehoeft, J.; Zeiser, C.; Haug, S.; Tempelaar, R.; Hestand, N. J.; Cerullo, G.; Broch, K. Modulating Singlet Fission by Scanning through Vibronic Resonances

in Pentacene-Based Blends. *J. Am. Chem. Soc.* **2022**, *144*, 20610−20619.
(13) Sayer, T.; Farah, Y. R.; Austin, R.; Sambur, J.; Krummel, A. T.; Montoya-Castillo, A. Trion Formation Resolves Observed Peak Shifts in the Optical Spectra of Transition-Metal Dichalcogenides. *Nano Lett.* **2023**, *23*, 6035−6041.
(14) Malý, P.; Lüttig, J.; Rose, P. A.; Turkin, A.; Lambert, C.; Krich, J. J.; Brixner, T. Separating Single- from Multi-Particle Dynamics in Nonlinear Spectroscopy. *Nature* **2023**, *616*, 280−287.
(15) Lüttig, J.; Rose, P. A.; Malý, P.; Turkin, A.; Bühler, M.; Lambert, C.; Krich, J. J.; Brixner, T. High-Order Pump−Probe and High-Order Two-Dimensional Electronic Spectroscopy on the Example of Squaraine Oligomers. *J. Chem. Phys.* **2023**, *158*, 234201.
(16) Lüttig, J.; Mueller, S.; Malý, P.; Krich, J. J.; Brixner, T. Higher-Order Multidimensional and Pump−Probe Spectroscopies. *J. Phys. Chem. Lett.* **2023**, *14*, 7556−7573.
(17) Mukamel, S. *Principles of Nonlinear Optical Spectroscopy*; Oxford Series in Optical and Imaging Sciences; Oxford University Press, 1999.
(18) Boyd, R. W. *Nonlinear Optics*; Academic Press: Burlington, 2008.
(19) Auston, D. H.; Shank, C. V.; LeFur, P. Picosecond Optical Measurements of Band-to-Band Auger Recombination of High-Density Plasmas in Germanium. *Phys. Rev. Lett.* **1975**, *35*, 1022−1025.
(20) Pedersen, S.; Baumert, T.; Zewail, A. H. Femtosecond Real-Time Probing of Reactions. 13. Multiphoton Dynamics of Mercury Iodide (IHgI). *J. Phys. Chem.* **1993**, *97*, 12460−12465.
(21) Bittner, T.; Irrgang, K.-D.; Renger, G.; Wasielewski, M. R. Ultrafast Excitation Energy Transfer and Exciton-Exciton Annihilation Processes in Isolated Light Harvesting Complexes of Photosystem II (LHC II) from Spinach. *J. Phys. Chem.* **1994**, *98*, 11821−11826.
(22) Smith, G. O.; Mayer, E. J.; Kuhl, J.; Ploog, K. Pump-Probe Investigations of Biexcitons in GaAs Quantum Wells. *Solid State Commun.* **1994**, *92*, 325−329.
(23) Valkunas, L.; Trinkunas, G.; Liuolia, V.; van Grondelle, R. Nonlinear Annihilation of Excitations in Photosynthetic Systems. *Biophys. J.* **1995**, *69*, 1117−1129.
(24) Yokoyama, K.; Silva, C.; Son, D. H.; Walhout, P. K.; Barbara, P. F. Detailed Investigation of the Femtosecond Pump-Probe Spectroscopy of the Hydrated Electron. *J. Phys. Chem. A* **1998**, *102*, 6957−6966.
(25) Klimov, V. I.; Mikhailovsky, A. A.; McBranch, D. W.; Leatherdale, C. A.; Bawendi, M. G. Quantization of Multiparticle Auger Rates in Semiconductor Quantum Dots. *Science* **2000**, *287*, 1011−1013.
(26) Brüggemann, B.; May, V. Exciton Exciton Annihilation Dynamics in Chromophore Complexes. II. Intensity Dependent Transient Absorption of the LH2 Antenna System. *J. Chem. Phys.* **2004**, *120*, 2325−2336.
(27) Ueda, A.; Matsuda, K.; Tayagaki, T.; Kanemitsu, Y. Carrier Multiplication in Carbon Nanotubes Studied by Femtosecond Pump-Probe Spectroscopy. *Appl. Phys. Lett.* **2008**, *92*, 233105.
(28) Hoffmann, M. C.; Hebling, J.; Hwang, H. Y.; Yeh, K.-L.; Nelson, K. A. THz-pump/THz-probe Spectroscopy of Semiconductors at High Field Strengths [Invited]. *J. Opt. Soc. Am. B* **2009**, *26*, A29−A34.
(29) Taguchi, S.; Saruyama, M.; Teranishi, T.; Kanemitsu, Y. Quantized Auger Recombination of Biexcitons in CdSe Nanorods Studied by Time-Resolved Photoluminescence and Transient-Absorption Spectroscopy. *Phys. Rev. B* **2011**, *83*, 155324.
(30) Tyagi, P.; Kambhampati, P. False Multiple Exciton Recombination and Multiple Exciton Generation Signals in Semiconductor Quantum Dots Arise from Surface Charge Trapping. *J. Chem. Phys.* **2011**, *134*, No. 094706.
(31) Almand-Hunter, A. E.; Li, H.; Cundiff, S. T.; Mootz, M.; Kira, M.; Koch, S. W. Quantum Droplets of Electrons and Holes. *Nature* **2014**, *506*, 471−475.
(32) Chen, L.; Palacino-González, E.; Gelin, M. F.; Domcke, W. Nonperturbative Response Functions: A Tool for the Interpretation of Four-Wave-Mixing Signals beyond Third Order. *J. Chem. Phys.* **2017**, *147*, 234104.
(33) Chlouba, T.; Trojánek, F.; Kopecký, V., Jr.; López-Vidrier, J.; Hernandéz, S.; Hiller, D.; Gutsch, S.; Zacharias, M.; Malý, P. Pathways of Carrier Recombination in Si/SiO2 Nanocrystal Superlattices. *J. Appl. Phys.* **2019**, *126*, 163101.
(34) Bressan, G.; van Thor, J. J. Theory of Two-Dimensional Spectroscopy with Intense Laser Fields. *J. Chem. Phys.* **2021**, *154*, 244111.
(35) Soni, A.; Kushavah, D.; Lu, L.-S.; Chang, W.-H.; Pal, S. K. Ultrafast Exciton Trapping and Exciton−Exciton Annihilation in Large-Area CVD-Grown Monolayer WS2. *J. Phys. Chem. C* **2021**, *125*, 23880−23888.
(36) Navotnaya, P.; Sohoni, S.; Lloyd, L. T.; Abdulhadi, S. M.; Ting, P.-C.; Higgins, J. S.; Engel, G. S. Annihilation of Excess Excitations along Phycocyanin Rods Precedes Downhill Flow to Allophycocyanin Cores in the Phycobilisome of Synechococcus Elongatus PCC 7942. *J. Phys. Chem. B* **2022**, *126*, 23−29.
(37) Kumar, S.; Dunn, I. S.; Deng, S.; Zhu, T.; Zhao, Q.; Williams, O. F.; Tempelaar, R.; Huang, L. Exciton Annihilation in Molecular Aggregates Suppressed through Quantum Interference. *Nat. Chem.* **2023**, *15*, 1118−1126.
(38) Hamm, P.; Zanni, M. *Concepts and Methods of 2D Infrared Spectroscopy*; Cambridge University Press: Cambridge, 2011.
(39) Knutson, J. R.; Beechem, J. M.; Brand, L. Simultaneous Analysis of Multiple Fluorescence Decay Curves: A Global Approach. *Chem. Phys. Lett.* **1983**, *102*, 501−507.
(40) Steinbach, P. J.; Ionescu, R.; Matthews, C. R. Analysis of Kinetics Using a Hybrid Maximum-Entropy/Nonlinear-Least-Squares Method: Application to Protein Folding. *Biophys. J.* **2002**, *82*, 2244−2255.
(41) van Stokkum, I. H. M.; Larsen, D. S.; van Grondelle, R. Global and Target Analysis of Time-Resolved Spectra. *Biochim. Biophys. Acta. Bioenerg.* **2004**, *1657*, 82−104.
(42) Rose, P. A.; Krich, J. J. Automatic Feynman Diagram Generation for Nonlinear Optical Spectroscopies and Application to Fifth-Order Spectroscopy with Pulse Overlaps. *J. Chem. Phys.* **2021**, *154*, No. 034109.
(43) Rose, P. A.; Krich, J. J. Numerical Method for Nonlinear Optical Spectroscopies: Ultrafast Ultrafast Spectroscopy. *J. Chem. Phys.* **2019**, *150*, 214105.
(44) Rose, P. A.; Krich, J. J. Efficient Numerical Method for Predicting Nonlinear Optical Spectroscopies of Open Systems. *J. Chem. Phys.* **2021**, *154*, No. 034108.
(45) Yuen-Zhou, J.; Krich, J. J.; Kassal, I.; Johnson, A. S.; Aspuru-Guzik, A. *Ultrafast Spectroscopy: Quantum Information and Wavepackets*; IOP Publishing, 2014.
(46) Yu, S.; Titze, M.; Zhu, Y.; Liu, X.; Li, H. Observation of Scalable and Deterministic Multi-Atom Dicke States in an Atomic Vapor. *Opt. Lett.* **2019**, *44*, 2795−2798.
(47) Abramavičius, D. Revealing a Full Quantum Ladder by Nonlinear Spectroscopy. *Lith. J. Phys.* **2020**, *60*, 154.
(48) Yang, L.; Mukamel, S. Revealing Exciton-Exciton Couplings in Semiconductors Using Multidimensional Four-Wave Mixing Signals. *Phys. Rev. B* **2008**, *77*, No. 075335.
(49) Malý, P.; Lüttig, J.; Turkin, A.; Dostál, J.; Lambert, C.; Brixner, T. From Wavelike to Sub-Diffusive Motion: Exciton Dynamics and Interaction in Squaraine Copolymers of Varying Length. *Chem. Sci.* **2020**, *11*, 456−466.

https://doi.org/10.1021/acs.jpclett.3c02491
J. Phys. Chem. Lett. 2023, 14, 10849−10855